JOURNAL OF GENERAL VIROLOGY

RESEARCH ARTICLE

Pacheco *et al.*, *Journal of General Virology* 2023;104:001838

DOI 10.1099/jgv.0.001838

MICROBIOLOGY SOCIETY

Digoxin is a potent inhibitor of Bunyamwera virus infection in cell culture

Beatriz Pacheco[1,2,*], Alberto Fernández-Oliva[1], Moisés García-Serradilla[1†] and Cristina Risco[1,*]

Abstract

Drug repurposing is a valuable source of new antivirals because many compounds used to treat a variety of pathologies can also inhibit viral infections. In this work, we have tested the antiviral capacity of four repurposed drugs to treat Bunyamwera virus (BUNV) infection in cell cultures. BUNV is the prototype of the *Bunyavirales* order, a large group of RNA viruses that includes important pathogens for humans, animals and plants. Mock- and BUNV-infected Vero and HEK293T cells were treated with non-toxic concentrations of digoxin, cyclosporin A, sunitinib and chloroquine. The four drugs inhibited BUNV infection with varying potency in Vero cells, and all except sunitinib also in HEK293T cells, with digoxin rendering the lowest half maximal inhibitory concentration (IC_{50}). Since digoxin rendered the best results, we selected this drug for a more detailed study. Digoxin is an inhibitor of the Na^+/K^+ ATPase, a plasma membrane enzyme responsible for the energy-dependent exchange of cytoplasmic Na^+ for extracellular K^+ in mammalian cells and involved in many signalling pathways. Digoxin was shown to act at an early time point after viral entry reducing the expression of the viral proteins Gc and N. Effects on the cell cycle caused by BUNV and digoxin were also analysed. In Vero cells, digoxin favoured the transition from G1 phase of the cell cycle to S phase, an effect that might contribute to the anti-BUNV effect of digoxin in this cell type. Transmission electron microscopy showed that digoxin impedes the assembly of the characteristic spherules that harbour the BUNV replication complexes and the morphogenesis of new viral particles. Both BUNV and digoxin induce similar changes in the morphology of mitochondria that become more electron-dense and have swollen cristae. The alterations of this essential organelle might be one of the factors responsible for digoxin-induced inhibition of viral infection. Digoxin did not inhibit BUNV infection in BHK-21 cells that have a digoxin-resistant Na^+/K^+ ATPase, which suggests that the effects of the blockade of this enzyme is a key factor of the antiviral activity of digoxin in BUNV-infected Vero cells.

INTRODUCTION

Emerging and reemerging viruses are a major health concern. In recent times, viruses such as Ebola virus (EBOV), influenza A virus (IAV), Dengue virus (DENV), Zika virus (ZIKV), Rift Valley Fever virus (RVFV), Crimean-Congo Haemorrhagic Fever virus (CCHFV), Lassa virus (LASV), Dabie bandavirus (DBV, former Severe Fever with Thrombocytopenia Syndrome virus, SFTSV), and several highly pathogenic coronaviruses (CoVs) are seriously challenging human health [1–8]. The 2019 outbreak of a novel coronavirus, SARS-CoV-2, originated a major pandemic that caused the death and threatened the life of millions of

Received 06 February 2023; Accepted 08 March 2023; Published 03 April 2023

Author affiliations: [1]Cell Structure Laboratory, National Center for Biotechnology, National Research Council, CNB-CSIC, Darwin 3, 28049 Madrid, Spain; [2]Department of Biochemistry and Molecular Biology, School of Pharmacy, Universidad Complutense de Madrid, Plaza Ramon y Cajal s/n, 28040 Madrid, Spain.

***Correspondence:** Beatriz Pacheco, b.pacheco@ucm.es; Cristina Risco, crisco@cnb.csic.es

Keywords: Bunyavirus; Bunyamwera virus; antiviral; drug repurposing; digoxin; cell cycle; mitochondria; Na^+/K^+ATPase.

Abbreviations: ATCC, American Type Culture Collection; BUNV, Bunyamwera virus; CC_{50}, 50 % cytotoxic concentration; CCHFV, Crimean-Congo Hemorrhagic Fever virus; CHIKV, Chikungunya virus; CoVs, coronaviruses; CQ, chloroquine; CsA, cyclosporine A; DAAs, direct-acting antivirals; DBV, Dabie bandavirus; DENV, Dengue virus; EBOV, Ebola virus; FBS, fetal bovine serum; Gc, BUNV large glycoprotein; GFP, green fluorescent protein; HCMV, human cytomegalovirus; HIV-1, human immunodeficiency virus type 1; h p.i., hours post-infection; IAV, influenza A virus; IC_{50}, half maximal inhibitory concentration; LASV, Lassa virus; m.o.i., multiplicity of infection; N, BUNV nucleocapsid protein; NSs, BUNV non-structural protein of the S segment; p.f.u., plaque forming units; PI, propidium iodide; rBUNGc-eGFP, chimeric fluorescent recombinant BUNV that expresses GFP fused to the Gc envelope glycoprotein; RVFV, Rift Valley Fever virus; SARS-CoV-2, severe acute respiratory syndrome coronavirus 2; TEM, transmission electron microscopy; WB, western blot; WT, wild type; ZIKV, Zika virus.

†Present address: Department of Anatomy and Embryology, School of Optics and Optometry, Universidad Complutense de Madrid, Plaza Ramon y Cajal s/n, 28040 Madrid, Spain.

Three supplementary figures are available with the online version of this article.

people worldwide. To combat present and future pandemics caused by pathogenic viruses, the validation of broad-spectrum antivirals that can be quickly applied to the clinic is a priority.

Broad-spectrum antivirals include two main categories: drugs targeting host-cell components essential for virus infection, and drugs directly targeting viruses [9]. Direct-acting antivirals (DAAs) usually are very potent. However, as they are designed to target a viral protein, DAAs are frequently very specific for the virus for which they were developed [10–13]. New antivirals can be found among the drugs used in the past to treat other pathologies. Repurposing of already approved drugs that target specific host factors commonly needed for several viruses can speed the process of developing broad-spectrum antivirals [12, 14–17].

Viruses are obligate intracellular parasites that need to hijack host-cell processes and pathways for their own replication. Interestingly, many viruses exploit common cellular pathways for their replication in the host cell. The identification of these cellular targets can be achieved by several experimental approaches that complement each other. Some studies apply genetic approaches, like RNA interference or CRISPR/Cas technologies, to identify cellular factors needed for viral replication [18, 19]. Biochemical methods have also been successful in identifying cellular proteins that directly interact with viral proteins [20]. Other studies have used high-throughput screenings (HTSs) to interrogate drug libraries for their ability to block viral infection in cell cultures [21, 22], and different microscopy techniques have been shown to be powerful tools to study virus–cell interactions and the mechanism of action of antiviral drugs [23–25].

Some of the most intriguing and important emerging and re-emerging viruses belong to the order *Bunyavirales,* which includes more than 500 species of viruses, some of which can cause severe disease in humans. The World Health Organization (WHO) has included CCHFV, LASV and RVFV, three members of the order *Bunyavirales*, in the list of prioritized infectious diseases. Other bunyaviruses, such as La Crosse, Hantaviruses and DBV (SFTSV) are important human pathogens. Although the concern about their current and future global impact is growing, there are no approved vaccines or therapies to combat bunyaviral infections [26], except for a hantavirus vaccine (Hantavax) approved in China and South Korea that has shown low efficacy.

In this study, we have used Bunyamwera virus (BUNV), the prototype virus of the *Bunyavirales* order, to analyse the antiviral potential of digoxin, sunitinib, chloroquine (CQ) and cyclosporin A (CsA), four drugs approved to treat heart conditions, cancer, malaria and for immune suppressive therapies, respectively. These drugs have shown potential for repurposing as broad-spectrum antivirals [12, 15, 16, 27], and have been tested against several viruses but not yet with bunyaviruses. We have found that these four compounds inhibit BUNV infection in cell cultures, with digoxin exhibiting the lowest IC_{50}. Our studies showed that digoxin impedes the assembly of viral replication organelles and new viral particles. This drug also caused a major transformation of the network of mitochondria, organelles that are recruited to viral factories assembled by many viruses, including bunyaviruses.

METHODS

Cell lines, drugs and viruses

Vero (CCL-81), HEK293T (CRL-3216), HeLa (CCL-2) and BHK-21 (CCL-10) cells were obtained from the American Type Culture Collection (ATCC) and maintained in DMEM supplemented with 10% fetal bovine serum (DMEM-10) and antibiotics.

The drugs used were: digoxin (D6003, Sigma), CQ (C6628, Sigma), CsA (120114, Abcam) and sunitinib malate (from now named 'sunitinib', PZ0012, Sigma).

Bunyamwera virus (VR-87) was obtained from the ATCC. Propagation and production of wild-type (WT) BUNV stocks was performed in Vero cells as previously described [28, 29]. The chimeric fluorescent recombinant virus rBUNGc-eGFP that expresses the green fluorescent protein (GFP) fused to the Gc envelope glycoprotein, was kindly provided by Dr R.M. Elliott (MRC-University of Glasgow Centre for Virus Research, UK) [30]. Virus titres (plaque forming units or p.f.u. per millilitre) were determined by standard plaque assay in Vero cells using an agar overlay [29].

Antibodies and fluorescence probes

The rabbit polyclonal antiserum against BUNV particles [29] and the mouse monoclonal antibody Mab742 specific for BUNV Gc protein [31] were kindly provided by Dr R.M. Elliott. The rabbit antiserum against BUNV N protein has been described previously [32]. The anti-β-actin monoclonal antibody (A5441) and the rabbit anti-TOMM22 antibody (HPA003037) were purchased from Sigma-Aldrich/Merck. Mitotracker Deep-Red 633 in DMSO (M22426) was obtained from Molecular Probes. DAPI (4′,6- diamidino-2-phenylindole) was obtained from Sigma-Aldrich.

Cytotoxicity assays

Cell cytotoxicity of the drugs was analysed with the MTT (3-[4,5-dimethylthiazol-2-yl]−2,5 diphenyl tetrazolium bromide) assay, which measures the mitochondrial dehydrogenase activity of living cells [33]. Cells were seeded in a 96-well plate at a density of 10 000 cells per well and incubated overnight at 37 °C with 5% CO_2. Cells were incubated with serial dilutions of the drugs in DMEM supplemented with 2% fetal bovine serum (DMEM-2) for 18 h followed by MTT solution (Sigma cat. no. M5655) at

0.5 mg ml^{-1} for 4 h at 37 °C with 5% CO_2 according to manufacturer instructions. The amount of MTT formazan formed was determined spectroscopically by measuring absorbance at 570 nm in an ELISA plate reader after dissolving the formazan crystals with MTT solvent (10% SDS, 0.01M HCl in 85% isopropanol).

Infections and inhibition assays with drugs

Cell monolayers at 80–90% confluency, were infected with rBUNGc-eGFP at a m.o.i. of 5 p.f.u. per cell in a small volume (450 µl per well for a 6-well plate) of DMEM-2 in the presence or absence of digoxin, CQ or CsA. Sunitinib emits fluorescence at the same wavelength as GFP, which limits the use of GFP fluorescence to measure the infectivity when cells are treated with this drug. Thus, the tests with sunitinib were done with the WT virus at a m.o.i. of 1 p.f.u. per cell. After 1 h of viral adsorption at 37 °C, viral inoculum was removed and replaced by fresh DMEM-2 medium with or without drugs. At 10 or 20 h post-infection (h p.i.) for the WT virus or rBUNGc-eGFP virus, respectively, the cells were lifted with 5 mM EDTA/PBS and fixed in 2% formaldehyde in PBS. Cells infected with WT virus were permeabilized with saponin and immunolabeled with rabbit anti-N serum and an anti-rabbit IgG conjugated to AlexaFluor647. The percentage of infected cells was determined by flow cytometry in a Beckman Coulter CYTOMICS FC 500 analyzer with CXP software or a BD LSRII Analyzer with DIVA software measuring Alexa Fluor 647 or GFP fluorescence for the WT or rBUNGc-eGFP viruses, respectively.

For the time-of-addition experiments to test the effect of the drugs at different steps of the infection, the drugs were added at selected time points before or after infection. To test the effect of the drugs at the entry step, drugs were added 3 h before infection and during virus adsorption (1 h), and afterwards removed from the medium (named '−3 h' time point). To test the effect of the drugs after the entry step, the drugs were added at 0, 1, 3 or 6 h after infection and maintained until cells were fixed with formaldehyde.

Western blots

Cells were infected with WT BUNV at 1 p.f.u. per cell in the presence or absence of 0.1 µM digoxin, a dose close to the IC_{50}, in six-well plates. Sixteen hours after infection cells were harvested with 5 mM EDTA in PBS and lysed with 40 µl of lysis buffer (1% NP-40, 0.1% SDS in PBS plus 2 mM EDTA, and a protease inhibitors cocktail). Cell lysates were analysed by SDS-PAGE and Western blot (WB) probing with an anti-BUNV antiserum (dilution 1:2000) and a secondary anti-rabbit IgG antibody conjugated to HRP (dilution 1:50 000) and visualized by ECL with a ChemiDoc Imager (BioRad). Blots were stripped and incubated with an anti-β-actin antibody (dilution 1:2000) and an anti-mouse IgG antibody conjugated to HRP (dilution 1:10 000). The relative amount of Gc and N viral proteins and cellular protein β-actin were quantified using Image Lab software (BioRad).

Analysis of cell cycle

To arrest the cell cycle at G0/G1, Vero and HEK293T (from now named 293T) cells were propagated in media without FBS for 24 h. To arrest the cycle at G2/M, cells were treated with 0.4 µg ml^{-1} of nocodazole for 8 h. After these treatments, cells were infected with rBUNGc-eGFP virus at 5 p.f.u. cell^{-1}. Sixteen hours after infection cells were collected with 5 mM EDTA in PBS and fixed and permeabilized with 100% methanol for 2 h on ice. After washing with PBS, cells were stained with propidium iodide (PI)/RNase staining buffer (BD Pharmingen, 550825) for 30 min. Analysis of PI fluorescence was performed in a Beckman Coulter CYTOMICS FC 500 flow cytometer with CXP software and doublet discrimination. PI fluorescence was collected in a linear scale and cell cycle phases calculated with FlowJo software cell cycle analysis tool.

Confocal and fluorescence microscopy

Vero cell monolayers were grown on glass coverslips and mock-infected or infected with WT BUNV at a m.o.i. of 1 p.f.u. cell^{-1}. At 1 h p.i., 0.1 µM digoxin was added to some cell cultures. At 8 h p.i., cells were collected, fixed 30 min with 4% paraformaldehyde in PBS, permeabilized with PBS containing 0.25% saponin and 2% FBS and processed for IF with primary and secondary antibodies diluted in PBS with 0.25% saponin and 2% FBS. To label the mitochondrial network, we used an anti-TOMM22 rabbit polyclonal antibody (1:200) and a secondary antibody conjugated with Alexa Fluor 594(1:500). The Gc viral glycoprotein was labelled with the mouse monoclonal antibody Mab742 diluted 1:200 and a secondary antibody conjugated with Alexa Fluor 488(1:500). Cells were stained with DAPI and mounted on glass slides with ProLong Gold Antifade Mountant (Molecular Probes). Images of at least 100 cells per condition were acquired with a Leica TCS SP5 confocal microscope.

Transmission electron microscopy

For ultrastructural studies, cells were processed as previously described [23, 34, 35]. Briefly, Vero cells were grown on sterile Thermanox Plastic Coverslips (Nunc) prior to infection. Monolayers of mock- and WT BUNV-infected cells were fixed with a mixture of 4% paraformaldehyde and 1% glutaraldehyde in HEPES 0.4 M, pH 7.4, for 1 h at room temperature. Samples were post-fixed 1 h at 4 °C with a mixture of 1% osmium tetroxide and 0.8% potassium ferricyanide in water, dehydrated at

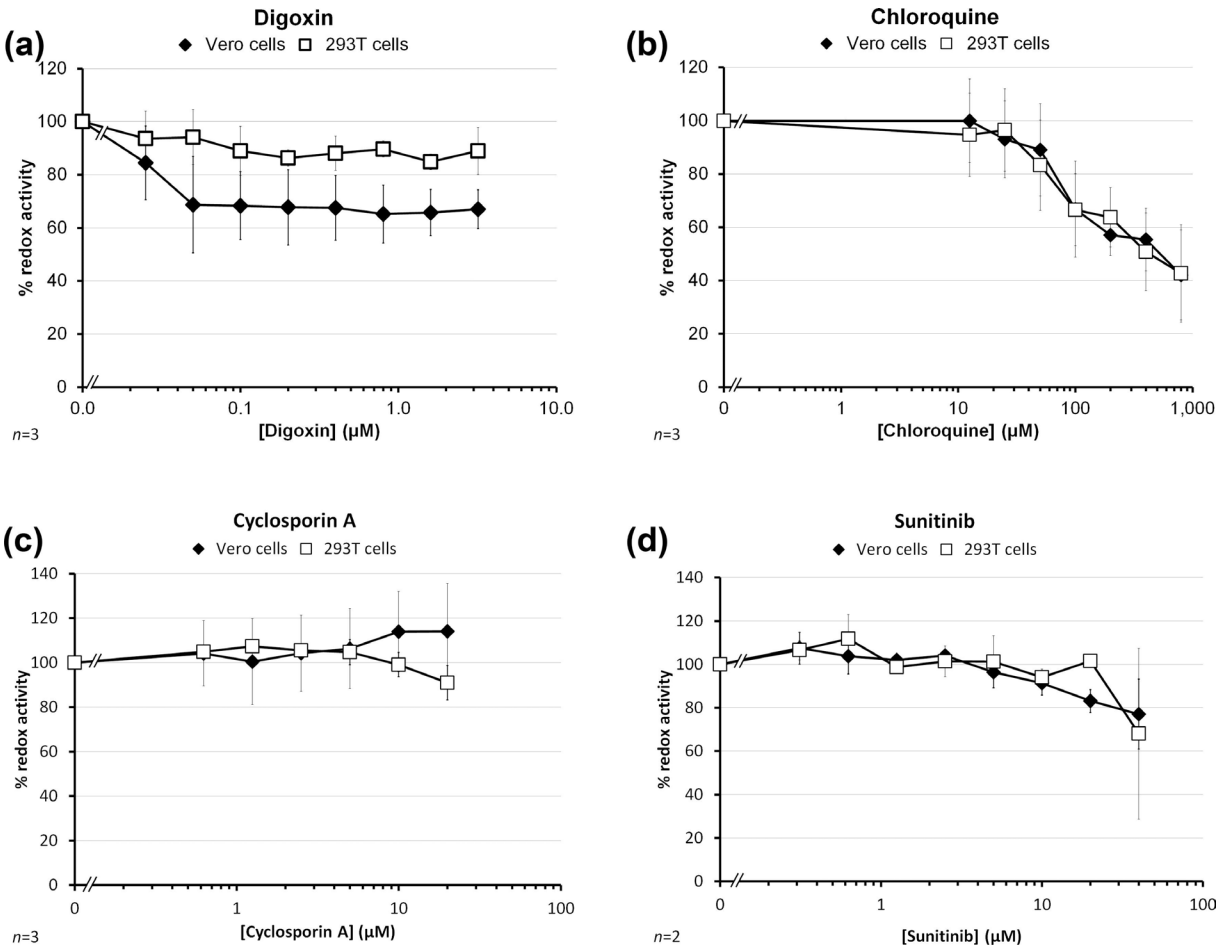

Fig. 1. Cytotoxicity assays with MTT of drugs in Vero and 293 T cells. A total of 10 000 cells per well were incubated with serial dilutions of the drugs for 18 h. Cells were then incubated with MTT solution for 4 h. The MTT crystal formed were dissolved with MTT solvent and the amount of MTT formazan formed was measured in an ELISA plate reader at 570 nm. The percentage of redox activity was calculated with respect to the control of untreated cells. The charts show the results of two or three independent experiments.

4 °C in 5 min steps with increasing concentrations of acetone (50, 70, 90% and twice in 100%), and embedded in the epoxy resin EML-812 (TAAB Laboratories). Samples were polymerized at 60 °C for 48 h. Ultrathin (~70–80 nm) oriented serial sections were obtained with a UC6 ultramicrotome (Leica Microsystems) and collected on uncoated 300-mesh copper grids (TAAB Laboratories). Sections were stained with saturated uranyl acetate and lead citrate and imaged by TEM. Images were acquired with a JEOL JEM 1011 electron microscope operating at 100 kV. At least 100 cells per condition were studied by electron microscopy.

Statistical analysis

For each experiment, at least two independent replicates were assessed. The significance levels (alpha) were set at 0.05, and the *P* values were calculated with a two-tailed *t*-test.

RESULTS

Cytotoxicity of drugs in cell culture

To assess the cytotoxic effects and the safe dose of the drugs in our cell culture system, we used the MTT assay (Fig. 1). This assay measures the mitochondrial dehydrogenase activity of living cells. Digoxin, CsA and sunitinib did not exhibit a substantial level of cytotoxicity at concentrations up to 3.2, 20 and 40 μM, respectively, both in Vero and 293 T cells. Additionally, no evidence of cell cytotoxicity was observed by phase contrast light microscopy (not shown). Since with digoxin in the Vero cells we observed a modest decrease in dehydrogenase activity using the MTT assay (approximately 30%, at the highest concentration tested), we decided to test cell viability using crystal-violet assay, which measures cell adhesion to the

plate and proliferation. In this assay we observed a reduction of approximately 20% of the cells attached to the plate at the highest concentrations (Fig. S1, available in the online version of this article), which might be due to a slower growth rate and/or a higher level of cell death. CQ reduced cell viability by about 50% at concentration above 400 µM using the MTT assay (Fig. 1), which was also evidenced by observation of the cells with a phase contrast light microscope (not shown). According to these results, an adequate range of concentrations was established for each compound to test the effect of the drugs in the progression of BUNV infection.

Inhibition of BUNV with drugs

Progression of BUNV infection in the presence of increasing concentrations of digoxin, CQ, CsA and sunitinib was studied in Vero and 293 T cells (Fig. 2). Considering that cell-type resistance to antivirals has been reported, using several cell lines of different origin is important for studying efficacy and potency of antiviral drugs [36]. The four drugs assessed in this study are established for use in a clinical setting for a long time, and although they have also shown their potential for drug repurposing as antivirals, they have not been tested against bunyaviruses [12].

The four drugs inhibited BUNV infection in Vero cells, calculated as the percentage of infected cells by flow cytometry (Fig. 2a). For these experiments, the fluorescent rBUNGc-eGFP recombinant virus was used [30]. The drugs exhibited different potency, with IC_{50} values of 74 nM for digoxin, 114 µM for CQ, >20 µM for CsA and 2.4 µM for sunitinib. We were unable to determine the exact IC_{50} of CsA due to the low solubility of this drug in the culture medium at concentrations above 20 µM. The results described above were obtained with the recombinant GFP virus. The N-terminal half of the Gc ectodomain has been shown to be dispensable for virus replication in cell culture [37]. In the recombinant virus used in this work the coding sequence of enhanced green fluorescent protein (eGFP) was fused to the N terminus of truncated Gc, and a recombinant BUNV (rBUNGc-eGFP) was rescued by reverse genetics [30]. The viability and autofluorescence of this recombinant virus indicated that chimeric Gc protein was functional and could fold correctly. Although the recombinant virus was attenuated in cell culture, it was competent to infect a wide range of cell lines as WT BUNV and was able to produce workable virus yields of 5×10^6 p.f.u. cell^{-1}. Although eGFP insertion usually causes attenuation, eGFP-recombinant viruses are useful for high-content screening of antiviral drugs [38], and have been used in several publications. To confirm that our results are not biassed by the use of the GFP recombinant virus, we infected Vero cells with WT BUNV and different concentrations of digoxin (Fig. S2A). The IC_{50} of digoxin determined with the WT BUNV (78 nM, Fig. S2A) and with the recombinant BUNV (74 nM, Fig. 1a) were very similar.

Vero cells are an African green monkey cell line commonly used to study BUNV and other viruses as well as for testing antivirals. To test the effect of the drugs in a human cell line, we infected 293 T cells in the presence or absence of the drugs (Fig. 2b). The inhibitory concentrations in 293 T cells were similar to those in Vero cells, with minor differences. Digoxin and CQ were somewhat less potent in 293 T cells compared to Vero cells with IC_{50} of 98 nM and about 200 µM, respectively. CsA was slightly more effective in 293 T cells with an IC_{50} of about 12.6 µM. However, sunitinib did not inhibit BUNV in 293 T cells at the concentrations tested. Digoxin was the most potent of all four drugs, with the lowest IC_{50} both in Vero and 293 T cells.

Results shown in Figs 1 and 2 suggest that part of the inhibitory activity of CQ against BUNV infection might be due to the cell cytotoxicity of the drug. In the case of digoxin, CsA, and sunitinib, their inhibitory effects are not attributable to cytotoxic effects in these cell lines. For CsA we were unable to calculate the *in vitro* selectivity index (ratio IC_{50}/CC_{50}) due to the low solubility of this drug at concentrations above 20 µM. However, for digoxin and sunitinib, the CC_{50} is higher than 3.2 and 40 µM, respectively, and we could estimate that the selectivity index *in vitro* is higher than 10, indicating that the antiviral effect of the drug is specific, and not due to cytotoxic effects.

Time-of-addition inhibition experiments

As digoxin was the drug with the highest antiviral activity, we decided to further characterize its mechanism of action. To elucidate which step of the viral cycle was affected by digoxin, we carried out infections with the recombinant virus adding this drug at different time points (Fig. 3). As previously reported, at 6 h p.i. the WT and recombinant BUNV have generated the first virus progeny [28, 30]. The time points used in this experiment were selected considering this replication kinetic of the virus. When adding digoxin up to 3 h p.i. it exerted its full activity, losing some inhibitory ability when added 6 h p.i. Similar results were obtained with the WT virus (Fig. S3). This suggests that digoxin exerts its antiviral effect at an early, post-entry time point of the infectious cycle, within the first 3–6 h of infection (Fig. 3).

Effect of digoxin on viral protein expression

To further characterize the mechanism of action of digoxin, its effect on the steady-state expression of N and Gc BUNV proteins was evaluated by Western blot with an anti-BUNV polyclonal antiserum that mainly recognizes the nucleocapsid protein (N) and the large glycoprotein (Gc) of BUNV (Fig. 4). For this study we used mock- and WT BUNV-infected Vero cells at 16 h p.i. because the peak of BUNV protein expression in this cell type infected at 1 p.f.u. cell^{-1} is detected from 12 to 20 h p.i. [39], coincident with the exponential phase of BUNV one step growth curves in Vero cells [28]. In Vero cells, at concentrations near the IC_{50}, digoxin

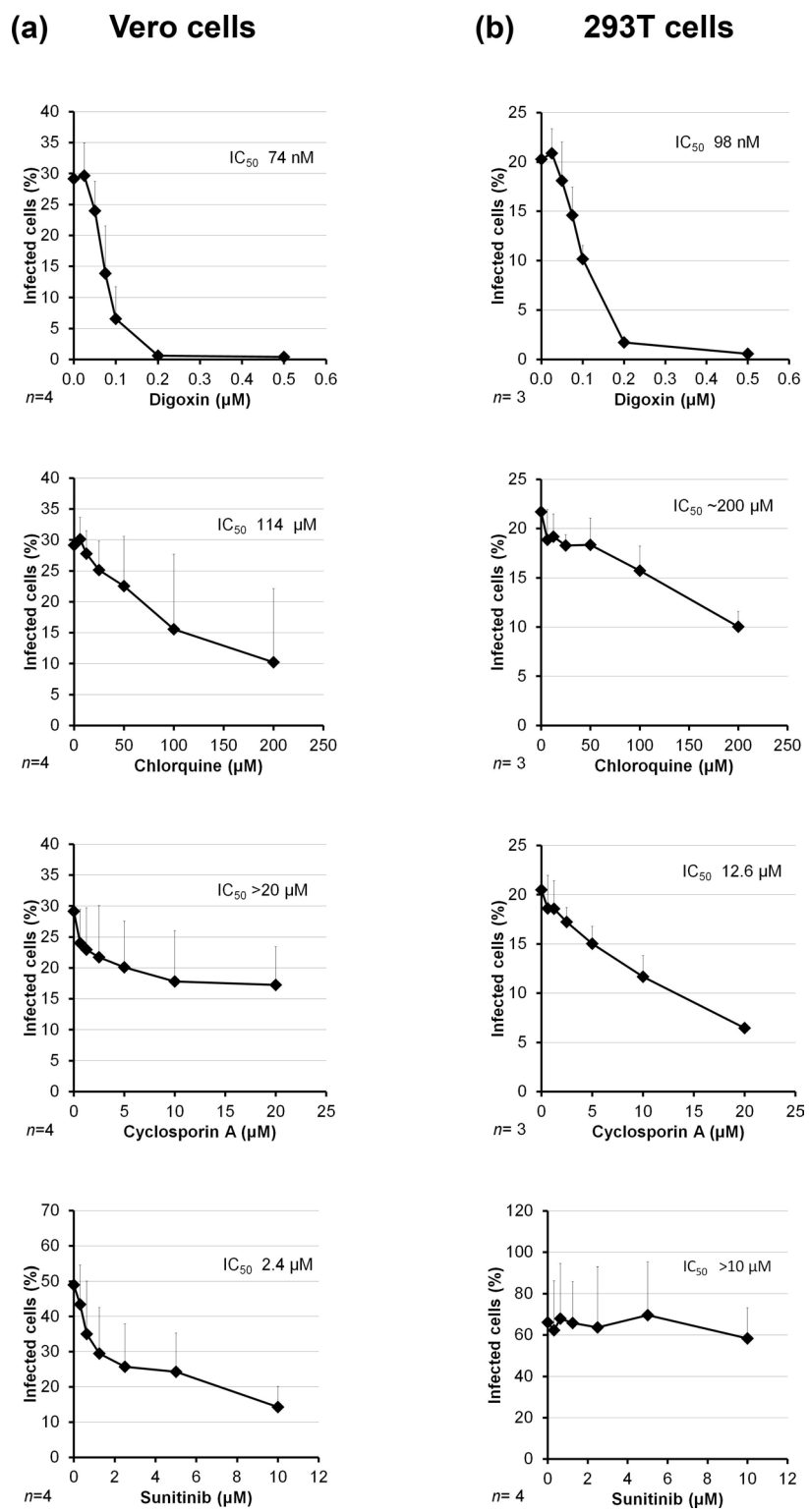

Fig. 2. Inhibition of BUNV infection with digoxin, chloroquine, cyclosporin A and sunitinib. Vero cells (a) and 293T cells (b) were infected with rBUNGc-eGFP at a m.o.i. of 5 p.f.u. per cell in the presence or absence of different concentrations of digoxin, CQ or CsA, or with the WT virus at a m.o.i. of 1 p.f.u. per cell and different concentrations of sunitinib. At 10 or 20 h p.i., for the WT virus or rBUNGc-eGFP virus, respectively, the percentage of infected cells was determined by flow cytometry as described in Methods. The charts show the results of three or four independent experiments. The mean percentage of infected cells+standard deviation of three or four independent experiments are shown.

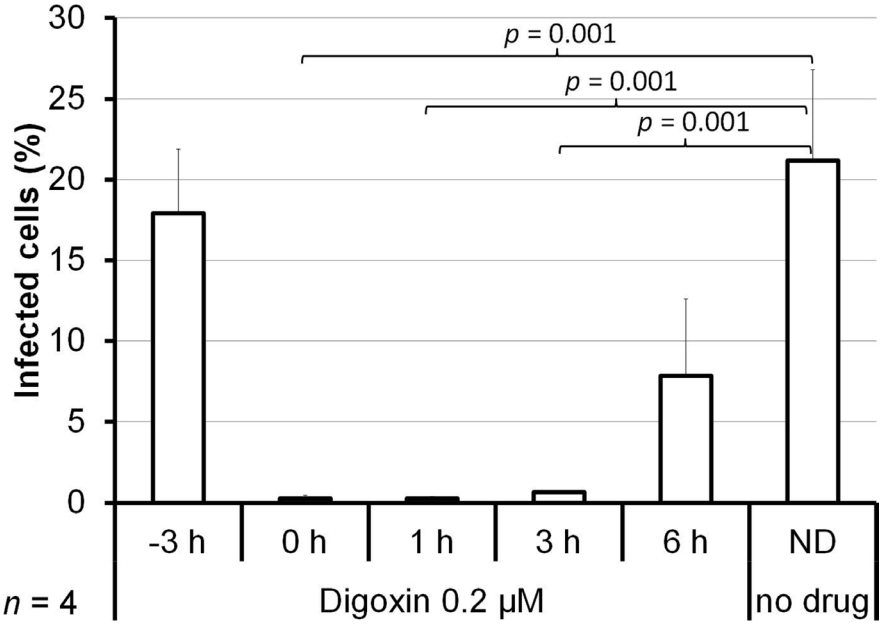

Fig. 3. Time-of-addition experiments of the inhibition of BUNV infection by digoxin in Vero cells. Cells were infected with rBUNGc-eGFP at a m.o.i. of 5 p.f.u. per cell. Digoxin was added at the indicated time points, 0, 1, 3 or 6 h p.i., and maintained for the rest of the time. For the time point '−3 h' the drug was added 3 h before infection and maintained during the 1 h of virus adsorption, afterwards the drug was removed. At 20 h p.i. the percentage of infected cells was determined by flow cytometry as described in Methods. The chart shows the results of four independent experiments. The mean percentages of infected cells+standard deviation of four independent experiments are shown. Reported *P* values (two-tailed) were calculated with Student's *t*-test.

significantly reduced the expression of N protein, that is expressed early in infection, and of glycoprotein Gc, that is expressed late in infection (Fig. 4a), in agreement with the results of viral infectivity shown in Fig. 2. In 293 T cells (Fig. 4b), we also observed a reduction of the production of viral proteins N and Gc with digoxin, although at lower levels than in Vero cells, in agreement with the lower activity of this drug in 293 T cells.

BUNV infection, digoxin and changes in cell-cycle phases

Some viruses have developed strategies to subvert the cell cycle for their own benefit, and create a cellular environment optimal for their replication [40]. To study whether BUNV replication is favoured by a specific phase of the cell cycle and how digoxin might affect this process, we studied changes in cell-cycle phases by flow cytometry. Cells were grown in media without FBS for 24 h (to arrest the cell cycle at G0/G1) or pre-treated with 0.4 µg ml^{-1} of nocodazole for 8 h (to arrest the cycle at G2/M). After these treatments, cells were infected with fluorescent rBUNGc-eGFP virus, fixed, stained with propidium iodide, and processed by flow cytometry. Results are shown in Fig. 5. In Vero cells, FBS starvation favoured BUNV infection, while nocodazole treatment was detrimental for the infection process (Fig. 5a). Nocodazole treatment also reduced BUNV infectivity in 293 T cells (Fig. 5a). However, FBS starvation reduced the percentage of 293 T cells infected by BUNV (Fig. 5a).

As the results in Vero and 293 T cells were apparently contradictory, we examined the effect that these treatments have in the cell cycle of non-infected cells (Fig. 5b). In Vero cells, FBS starvation and nocodazole treatment induced an arrest in G0/G1 and G2/M, respectively, as expected. In 293 T cells, nocodazole also arrested cell cycle at G2/M. However, FBS starvation did not have a significant effect on the cell cycle in 293 T cells (Fig. 5b), which could explain the negative effect that the lack of FBS has on BUNV infection in these cells. It has been reported that SV40 large T antigen present in the 293 T cells is implicated in cell transformation, overriding cell-cycle check points by different mechanisms, and driving cells into S-phase [41], in agreement with our data of the effect of FBS starvation in the cell cycle of 293 T cells (Fig. 5b).

Our data suggest that BUNV infection in Vero cells is favoured when cells are arrested in G0/G1 phase. In addition, the lower percentage of cells in G0/G1 phase in the 293 T cells compared with Vero cells could also account for the lower infectivity of BUNV in 293 T cells compared with Vero cells.

To test if BUNV infection was able to induce cell-cycle arrest in G0/G1, we infected Vero and 293 T cells with the recombinant BUNV and analysed changes in cell-cycle phases by flow cytometry. In Vero cells, BUNV infection did not appear to affect cell cycle (Fig. 5c). However, we observed a modest increase (from 46–54%) in the percentage of cells in G0/G1 phase in

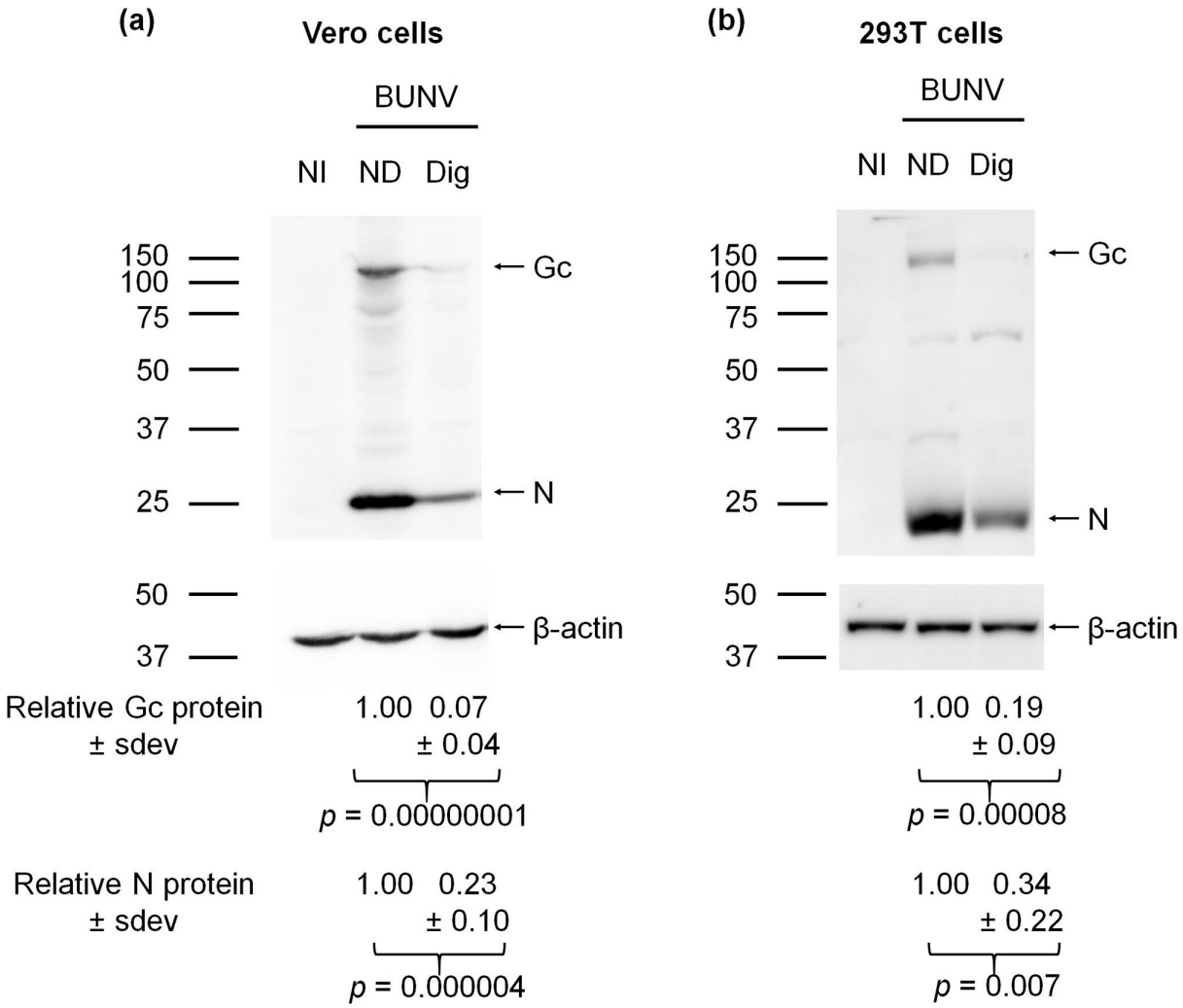

Fig. 4. Effect of digoxin on viral protein expression. Vero (a) and 293T (b) cells were infected with WT BUNV at 1 p.f.u. per cell in the presence or absence of 0.1 µM digoxin. Sixteen hours after infection cells were lifted with EDTA and analysed by WB with antiBUN (dilution 1:2000) or anti*β*actin (dilution 1:2000) antibody. NI, noninfected; ND, no drug; Dig, digoxin. One experiment representative of four (Vero cells) or three (293T cells) is shown. The numbers below the gels show the average relative quantity of the Gc protein/*β*-actin and N protein/*β*-actin±standard deviation for all the experiments. The *P* values (two-tailed) were calculated with Student's *t*-test.

the 293 T cells infected with BUNV (Fig. 5c). Similar results were obtained when the cells were seeded at low density (data not shown). Our experiments of infection had been undertaken at a relatively high confluency and with a low percentage of FBS, which could have masked the results of cell cycle. To clarify whether BUNV infection affects the cell cycle in Vero cells, we starved the cells for 48 h in media without FBS to synchronize the cells at G0/G1. Then we added DMEM with 10% FBS and infected the cells with BUNV. We collected the cells at 0 and 16 h after infection and analysed the cell cycle. In these conditions we observed that the mock infected cells entered the cell cycle again and recovered after 16 h, while most BUNV-infected cells remained in G0/G1 phase (Fig. 5d), suggesting that BUNV arrests cells at G0/G1.

To study whether part of the antiviral effect of digoxin could be due to its effect in the cell cycle, we treated the cells with the drug and analysed the changes in the cell-cycle phases. Treatment of Vero cells with digoxin favoured the transition from G1 to S phase (Fig. 6), which could in part explain the reduction in viral replication in the presence of digoxin, as we have observed that viral replication is favoured in G0/G1 phase.

Effect of BUNV infection and digoxin on viral structures and cell compartments

We also studied the effects of digoxin on key events of viral infection with the help of light and electron microscopy.

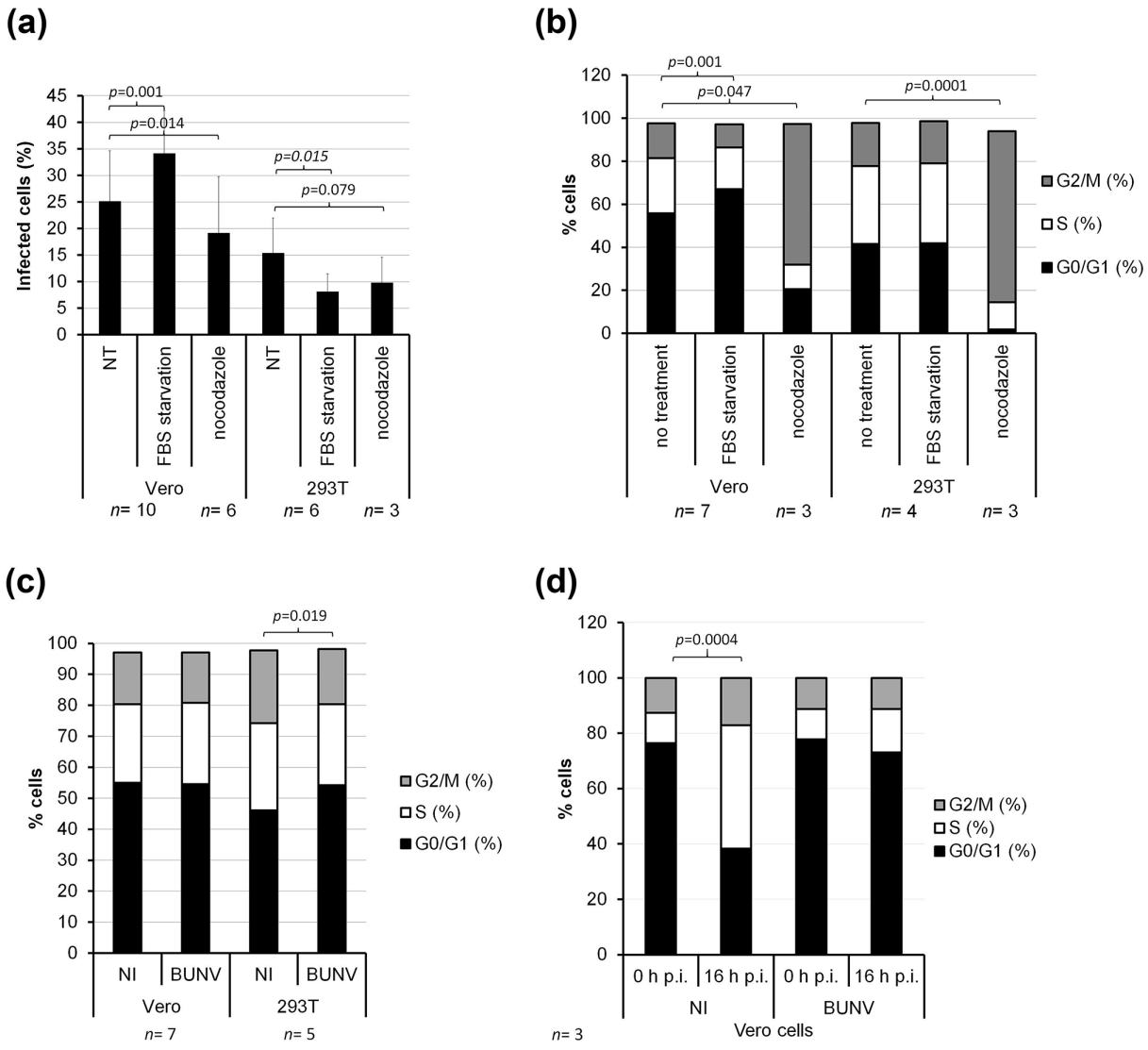

Fig. 5. BUNV infection and changes in cell-cycle phases. Effect of cell-cycle arrest on BUNV infection (a) and the cell-cycle phases (b), and effect of BUNV infection in the cell cycle of unsynchronized cells (c) and synchronized cells (d). Cells were grown for 24 h in media with FBS (NT), or media without FBS (FBS starvation) or treated with nocodazole for 8 h (nocodazole), and then infected with rBUNGc-eGFP at a m.o.i. of 5 p.f.u. per cell in DMEM-2. Sixteen hours post-infection the percentage of infected cells was determined by flow cytometry (a). (b) Cells were treated as in (a) and mock infected, and the phase of cell cycle was determined with PI. (c) Cells were grown in DMEM-2 and mock infected or infected with rBUNGc-eGFP at a m.o.i. of 5 p.f.u. per cell. Sixteen h p.i. cell cycle was analysed by flow cytometry with PI staining. (d) Vero cells were grown in media without FBS for 48 h to synchronize them at G0/G1, and then the cells were infected as above in DMEM-10. Sixteen h p.i. the cell cycle was analysed by staining with PI. The *P* values (two-tailed) were calculated with Student's *t*-test.

To study the effects of digoxin on the assembly of BUNV replication organelles and viral particles, Vero cells were mock- or WT BUNV-infected in the presence or absence of digoxin before chemical fixation, processing for embedding in resin, ultra-microtomy and transmission electron microscopy (TEM) (Figs 7 and 8). In BUNV-infected Vero cells, the Golgi complex is fragmented and contains spherules, that are the structures harbouring the viral replication complexes, as well as viral particles (Fig. 7a, b) [28]. In BUNV-infected Vero cells treated with digoxin, the Golgi complex is not fragmented, and spherules and viral particles are absent (Fig. 7c, d). When studying the effects on cell organelles, the most striking changes induced by either BUNV infection or digoxin were detected in the mitochondrial network (Fig. 8). In mock-infected cells, mitochondria have a characteristic elongated shape and well defined, parallel cristae (Fig. 8a). In BUNV-infected cells, mitochondria exhibit a higher electron-density, and swollen cristae (Fig. 8b). In mock-infected, digoxin-treated cells, mitochondria exhibit a similar morphology than in BUNV-infected cells: they are electron-dense and contain swollen cristae (Fig. 8c). In Vero cells infected with BUNV and treated with digoxin, mitochondria have a different morphology: a few cristae are observed in some of

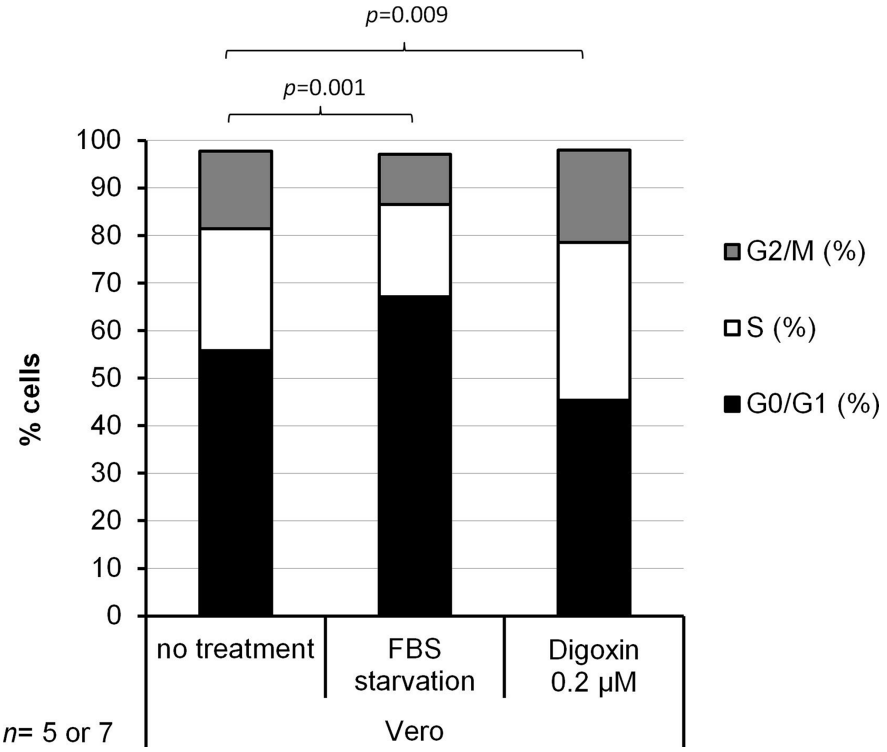

Fig. 6. Effect of digoxin treatment in the Vero cell cycle. Vero cells were left untreated or treated with media without FBS for 24 h or with digoxin for 18 h. Afterwards, cells were lifted and stained with PI to analyse the cell-cycle phases. The chart shows the mean percentage of cells in each phase of the cell cycle of five or seven independent experiments. The *P* values (two-tailed) were calculated with Student's *t*-test.

them, but most mitochondria do not have characteristic cristae (Fig. 8d). Higher magnification views of mitochondria from these four different conditions are shown in Fig. 8e–h. A quantitative analysis of mitochondria morphologies based on the observation of 1148 mitochondria from 49 sectioned cells is shown in Table 1.

To further characterize changes in mitochondrial networks, cells were processed by immunofluorescence and analysed by confocal microscopy (Fig. 9). In mock-infected cells, the network of mitochondria extends from the nucleus to the periphery of the cell and individual mitochondria have similar morphology and dimensions throughout the cell (Fig. 9a). However, in BUNV-infected cells, mitochondria are massively recruited and aggregated near the nucleus where they associate to Gc-containing viral factories, with few mitochondria on the cell periphery (Fig. 9b). Interestingly, in mock-infected cells treated with digoxin, mitochondria are also aggregated near the nucleus, while on the cell periphery they appear small and highly fragmented (Fig. 9c). In the presence of BUNV and digoxin, Vero cells show a general fragmentation of the mitochondrial network, as well as aggregation of mitochondria, partially coincident with viral factories (Fig. 9d).

In conclusion, results obtained by electron and confocal microscopy suggest that both BUNV and digoxin alter mitochondria, and that digoxin might be interfering with essential steps of viral replication that depend on this organelle.

Digoxin does not inhibit BUNV infection in BHK-21 cells

To investigate whether the inhibition of the Na^+/K^+ ATPase by digoxin might play a key role in the capacity of the drug to inhibit BUNV infection, we studied the effects of digoxin in BUNV-infected BHK-21 cells and in parallel in Vero cells. The Vero and BHK-21 cells were infected with wild-type BUNV (Fig. S2A, B, respectively). Cardiac glycosides inhibit the Na^+/K^+ ATPase through binding to the catalytic subunit but do so with less efficiency to specific mice, rat and hamster isoforms relative to their human counterparts [42, 43]. For example, the rat Na^+/K^+ ATPase has several mutations that render the enzyme insensitive to ouabain (Fig. S2C) [44] and presumably, to other similar cardiac glycosides such as digoxin (Fig. S2D). In inhibition assays, digoxin blocked BUNV infection in Vero cells at non-toxic concentrations, with an IC_{50} of 78 nM (Fig. S2A). However, digoxin did not inhibit BUNV infection in BHK-21 cells (Fig. S2B), whose Na^+/K^+ ATPase shares key mutations with the rat ATPase catalytic subunit (Fig. S2C).

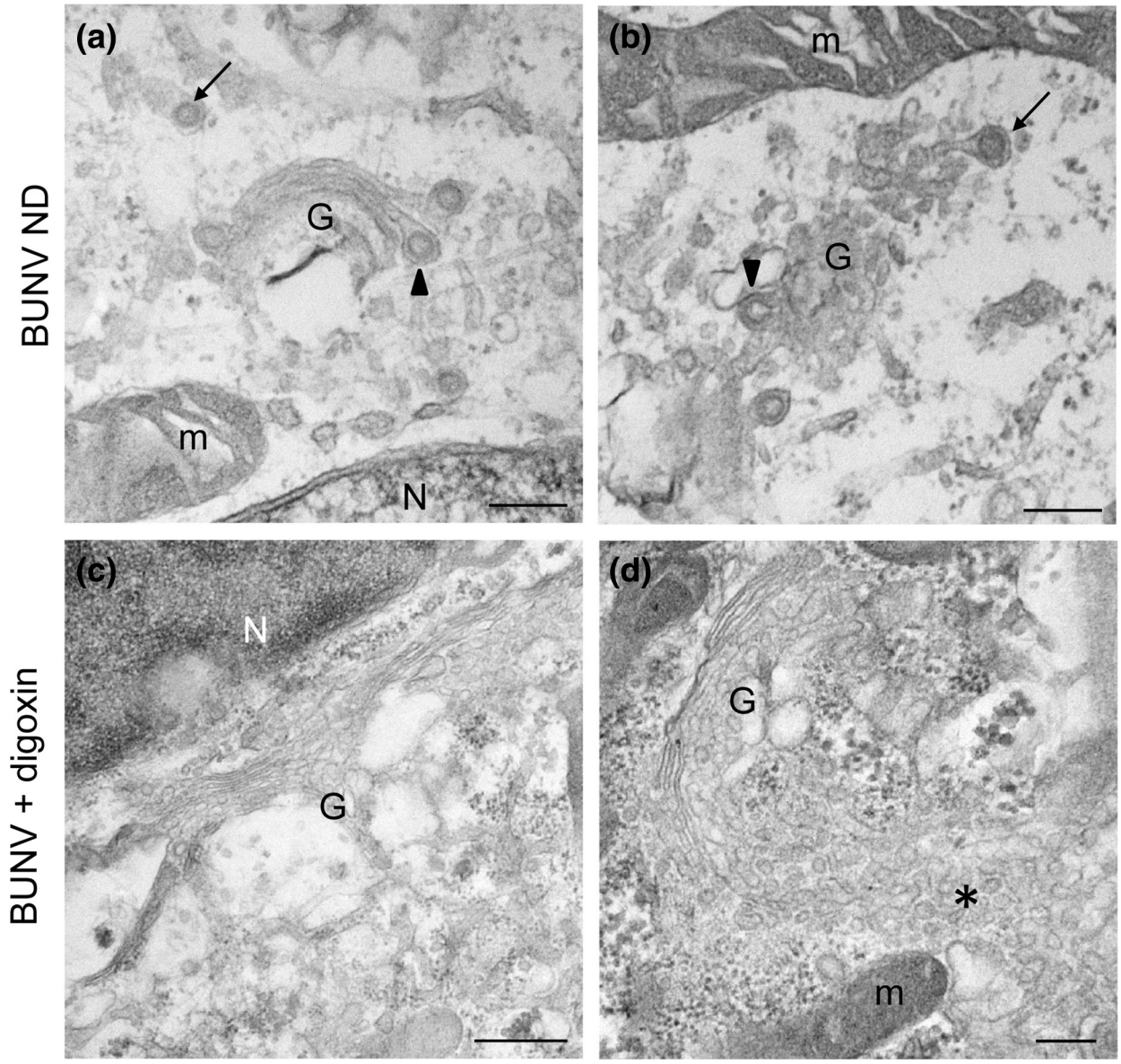

Fig. 7. Electron microscopy of BUNV-infected Vero cells, in the presence and absence of digoxin. Cells were infected with WT BUNV at a m.o.i. of 1 p.f.u. cell^{-1}. At 1 h p.i., 0.1 µM digoxin was added to some cell cultures as indicated. At 8 h p.i., cells were collected and processed for embedding in an epoxy-resin, ultramicrotomy and TEM. (a) and (b) The Golgi complex (G) of BUNV-infected Vero cells contains characteristic spherules (arrowheads) and viral particles (arrows). (c) and (d) The Golgi complex of BUNV-infected Vero cells treated with digoxin do not have viral structures. N, nucleus; m, mitochondrion; asterisk, groups of vesicles. Scale bars: 200 nm in (a), (b) and (d); 0.5 µm in (c).

DISCUSSION

In recent years, there has been an increased interest in obtaining drugs to treat many viral infections. There is a long list of drugs, already approved for the treatment of different diseases, which have shown promising results for repurposing as broad-spectrum antivirals [12, 15, 16, 27]. Here we have studied the antiviral activity against BUNV of digoxin, chloroquine, cyclosporine A and sunitinib, drugs that are currently included in clinical trials to treat a variety of pathologies, including viral infections (https://clinicaltrials.gov). However, to our knowledge, they have not been previously tested to treat bunyavirus infections. In the present work, we have found that the four drugs inhibited BUNV replication with different potency in Vero cells and all but sunitinib, also in 293 T cells, with digoxin presenting the lowest IC_{50} in both cell types.

Digoxin is a cardiac glycoside used to treat certain heart conditions. In cell culture, digoxin has been shown to inhibit several viruses, like CHIKV (IC_{50} 67 nM) [42], SARS-CoV-2 (IC_{50} 43 nM and 190 nM) [45, 46], HCMV (IC_{50} 36 nM) [47] or HIV-1

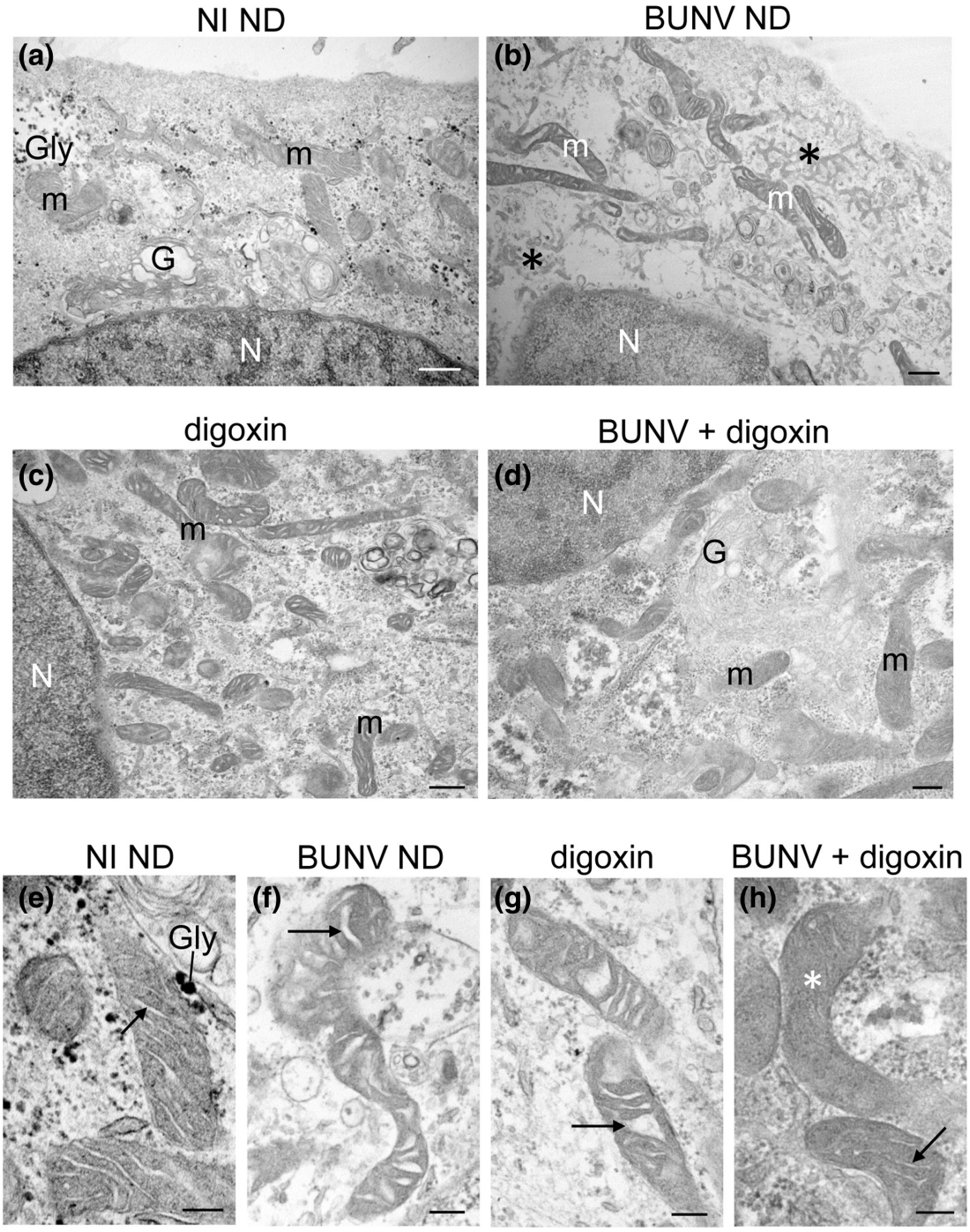

Fig. 8. Electron microscopy of the mitochondrial network in mock- and BUNV-infected Vero cells, in the presence and absence of digoxin. Cells were mock-infected or infected with WT BUNV at a p.f.u. cell^{-1} of 1 p.f.u. cell^{-1}. At 1 h p.i., 0.1 µM digoxin was added to some cell cultures as indicated. At 8 h p.i., cells were collected and processed for embedding in an epoxy-resin, ultramicrotomy and TEM. (a) Mock-infected cells contain elongated mitochondria (m) of medium electron-density, characteristic Golgi stacks (G) and glycogen granules (Gly). (b) BUNV-infected cells contain electron-dense mitochondria with swollen cristae and disrupted/fragmented membranes (asterisks). The cytosol has low electron density. Intact Golgi stacks and glycogen granules are not observed. (c) Mock-infected cells incubated with digoxin contain a normal cytosol and electron-dense mitochondria with swollen cristae. Glycogen granules are not observed. (d) BUNV-infected cells treated with digoxin contain a normal cytosol, intact Golgi stacks and mitochondria with few cristae. (e) to (h) High-magnification images of mitochondria in cells from the four described conditions. Arrows point to mitochondrial cristae. The white asterisk in (h) marks a mitochondrion with few cristae. NI, non-infected cells. ND, no drug treatment. N, nucleus. Scale bars, 0.5 µm in (a) to (d); 200 nm in (e) to (h).

Table 1. TEM quantitative analysis of mitochondria morphologies in mock- or BUNV-infected Vero cells, with or without digoxin. Quantification was based on the observation of 1,148 mitochondria from 49 sectioned cells processed as described in Fig. 9. For non-infected cells without digoxin (NI ND), a total of 128 mitochondria from ten sectioned cells were studied. For non-infected Vero cells treated with digoxin (NI + Digoxin), we studied 378 mitochondria from 11 sectioned cells. For BUNV-infected Vero cells without digoxin (BUNV ND) we studied 267 mitochondria from ten sectioned cells. For BUNV-infected Vero cells treated with digoxin (BUNV + Digoxin) 267 mitochondria from 10 sectioned cells were studied. Percentage (%) of cells corresponding to one of the four described morphologies (normal, resting; normal, active; abnormal swollen cristae; abnormal, few cristae) are shown

Treatment	Normal resting mitochondria 	Normal active Mitochondria 	Abnormal mitochondria swollen cristae 	Abnormal mitochondria few cristae 
NI ND	92.2 %	6.3 %	1.5 %	-
NI + digoxin	-	6.6 %	84.7 %	8.7 %
BUNV ND	0.4 %	0.4 %	99.2%	-
BUNV + digoxin	-	2.4 %	2.6 %	95.0%

(IC_{50} 45 nM) [48, 49]. These IC_{50} values are similar to those found for BUNV in this work (IC_{50} 74 and 98 nM in Vero and 293 T cells, respectively).

Although digoxin inhibited BUNV replication in cell culture, it did so at concentrations above those acceptable for treatment. The therapeutic serum concentrations of digoxin for the treatment of heart disease range from 0.6 to 2.6 nM, and the toxic level is established above 3 nM, which is clearly lower than the effective concentrations that inhibit BUNV replication in cell culture (IC_{50} 74 and 98 nM for Vero and 293 T cells, respectively) (Fig. 2). Thus, development of less toxic derivatives would be necessary before cardiac glycosides can be used as antivirals in the clinic. A possible solution to this limitation is the design of treatments with cocktails of drugs used at low concentrations. Apart from reduced toxicity, combined therapies with several drugs have better efficacy and prevent the development of resistant viral strains [50]. Although interfering with cellular factors and pathways can cause unwanted side effects, many diseases are currently treated by targeting a host function. For these treatments, pharmaceutical companies have developed compounds and adequate dose regimes that are well tolerated by patients. Shortening the duration of therapies from months or years to several days or a few weeks should also help to limit toxicity [51].

Digoxin could inhibit BUNV infection through several mechanisms. In our cell cultures we did not observe significant cytotoxic effects at the concentrations that inhibit viral replication, which indicates that digoxin inhibition of BUNV replication is not due to cytotoxicity. Our data show that digoxin acts after viral entry and disrupts the replication cycle of BUNV reducing the amount of viral proteins, which points to an early effect of the drug in one or more steps of the virus life cycle. We have observed that digoxin impairs the assembly of BUNV replication organelles and the morphogenesis of viral particles in the Golgi complex, and also blocks the characteristic fragmentation of this organelle previously reported for BUNV-infected Vero cells [28]. Previous studies have shown that digoxin and other cardiac glycosides can impair viral replication by altering cell signalling mediated by Na^+/K^+ ATPases and affecting the synthesis of viral proteins and vRNA [52]. Here we show that digoxin might also affect viral replication by altering the cell cycle and the mitochondrial network structure, an effect that to our knowledge has not been reported before.

Some viruses have developed strategies to subvert the cell cycle in their own benefit and create a cellular environment optimal for their replication, frequently deregulating specific cell-cycle checkpoints [40]. In this work, we have observed that BUNV replication is favoured when the cell cycle is arrested in G0/G1. The BUNV non-structural protein NSs could be implicated in this process. NSs, the only bunyavirus protein known to reach the nucleus, is a viral interferon antagonist that counteracts the host viral response to infection, induces DNA damage responses, cell-cycle arrest at the S or G0/G1 phase and protein synthesis shut-off [53–56]. Arrest at G0/G1 phase may facilitate viral protein synthesis and avoid competition for cellular DNA replication machinery. Our studies suggest that BUNV infection arrest the cell cycle at G0/G1 (Fig. 5c, d). In contrast,

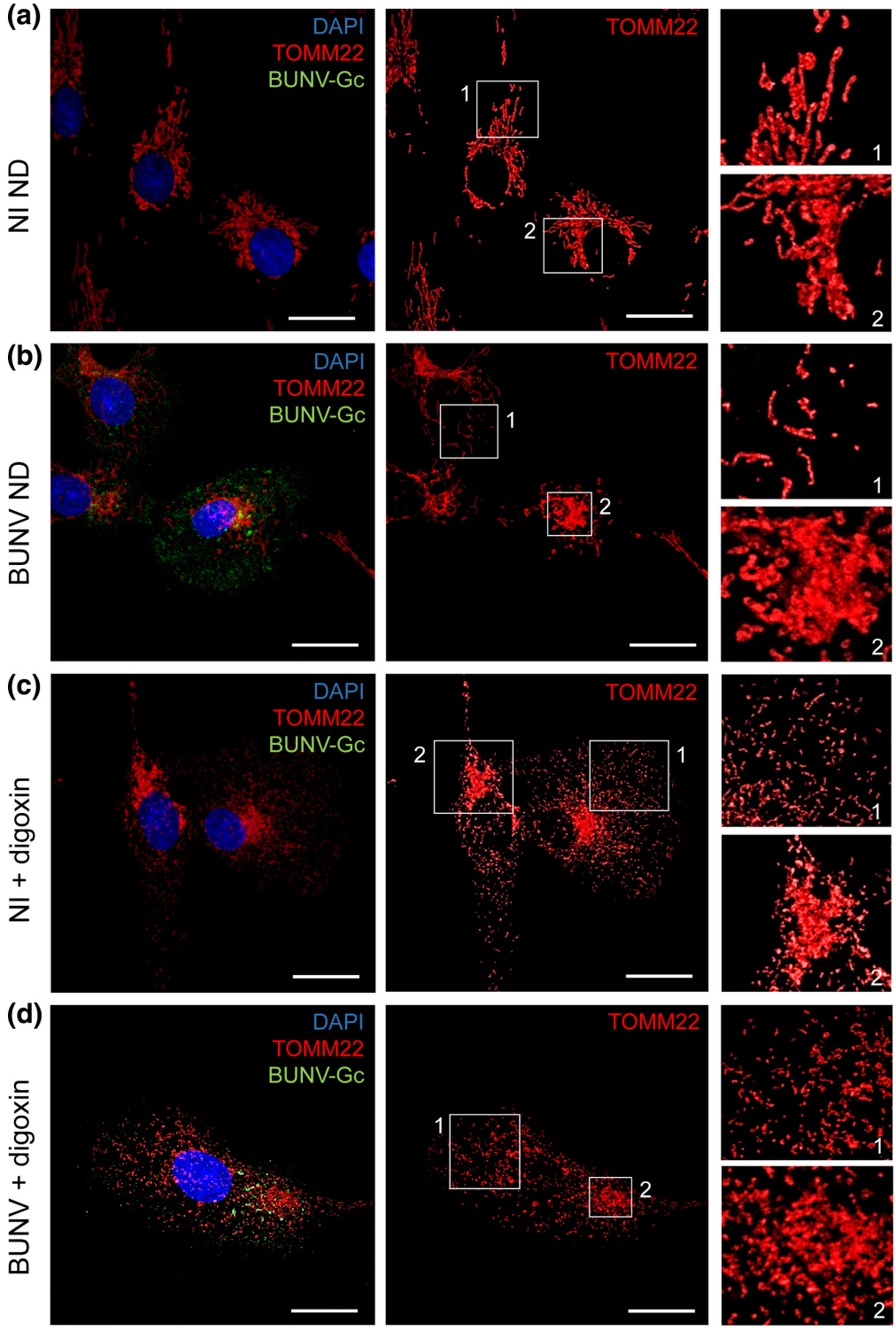

Fig. 9. Confocal microscopy of the mitochondrial network in mock- and BUNV-infected Vero cells, in the presence and absence of digoxin. Cells were mock-infected or infected with WT BUNV at a m.o.i. of 1 p.f.u. cell^{-1}. At 1 h p.i., 0.1 µM digoxin was added to some cell cultures, as indicated. At 8 h p.i., cells were collected and processed for IF with a rabbit anti-TOMM22 polyclonal antibody that labels the mitochondrial network and a secondary antibody conjugated with Alexa Fluor 594 (red). The Gc viral glycoprotein was labelled with a mouse monoclonal antibody and a secondary antibody conjugated with Alexa Fluor 488 (green). Nuclei were stained with DAPI (blue). The general view of cells with their whole mitochondrial network (images on the left and centre) is accompanied by zooms of peripheral (1) and juxtanuclear (2) mitochondria (images on the right). NI, non-infected cells. ND, no drug treatment. Scale bars, 25 µm.

digoxin favoured the transition from G1 to S phase of the cell cycle in Vero cells, which might participate in the antiviral effect of digoxin in this cell line.

Many RNA viruses hijack mitochondria early in infection. In fact, recruitment of mitochondria to viral factories is one of the characteristic features of virus factory assembly [57]. Although the specific roles of mitochondria in viral infections have not been fully elucidated, it is known that viruses interact with mitochondria in different ways and at different moments of their life cycle [32, 58–61]. TEM of mock-infected cells has shown different morphologies for normal resting mitochondria, compared to normal actively respiring mitochondria [62–64]. TEM has also shown that viruses induce changes in the morphology and intracellular location of mitochondria [32, 57, 59]. Here we show that in BUNV-infected Vero cells, mitochondria exhibited an altered morphology with swollen cristae.

Mitochondria are highly dynamic organelles that participate in numerous cellular functions. To meet the needs of the cell, mitochondria are able to constantly change their shape and size through fission and fusion processes that are important for correct mitochondrial function and cell survival. In addition to their role in ATP generation, mitochondria are implicated in several cellular functions including apoptosis and signal transduction in the innate immune response [65], as well as cell-cycle control [66, 67]. Viruses can affect mitochondria, altering their metabolism and energy generation [60], and blocking the mitochondrial-mediated antiviral response [58]. In addition, viruses can also use mitochondrial proteins. For example, interactions between the mitochondrial protein p32 and a number of viral proteins are important for virus replication [68]. Although the specific role of mitochondria in bunyavirus infection and digoxin treatment remains to be fully defined, we propose that both BUNV and digoxin alter mitochondria directly or indirectly and that mitochondria alterations induced by digoxin might interfere with essential steps of viral infection.

As mentioned previously, digoxin blocks the Na^+/K^+ ATPase, which is essential for most cells [69]. This membrane-bound enzyme is responsible for the energy-dependent exchange of cytoplasmic Na^+ for extracellular K^+ in mammalian cells [70]. The anti-BUNV effect of digoxin might be related to alterations of Na^+, K^+ and Ca^{2+} flows. It has been shown that inhibition of the Na^+/K^+ ATPase can impair mitochondrial energetics and induce abnormal Ca^{2+} cycling increasing intracellular Ca^{2+} levels [71, 72]. High intracellular levels of Ca^{2+} or K^+ cause mitochondria swelling [73, 74], which might account for the digoxin-induced alterations in the mitochondrial network. Interestingly, in BUNV-infected cells and mock cells treated with digoxin the alterations in mitochondrial ultrastructure were similar, presenting high electron-density and swollen cristae. The bunyavirus DBV induces an increase in the intracellular levels of Ca^{2+} and the blockade of Ca^{2+} channels inhibits DBV infection [8]. Also, BUNV needs high K^+ levels inside endosomes for releasing its genome into the cytosol [75, 76]. The digoxin-induced blockade of the Na^+/K^+ ATPase would reduce the intracellular K^+ levels and make the release of BUNV virions from endosomes to cytosol less efficient, impairing infection. This potential mechanism of action for cardiac glycosides has also been proposed for other viruses [42, 77]. In our case, the lack of antiviral activity of digoxin in BUNV-infected BHK-21 cells (Fig. S2) suggests that the blockade of Na^+/K^+ ATPase is a key cell factor of the antiviral activity of digoxin in BUNV-infected Vero cells. Together with coronaviruses, reoviruses, herpesviruses, alphaviruses and flaviviruses [77], bunyaviruses can be now added to the list of viruses inhibited by cardiac glycosides. Inhibition of the sodium-potassium ion pump can affect many cellular signalling pathways [78]. In our study, we have observed changes in the cell cycle and mitochondria that, together with alterations of ion flows, might cause the digoxin-induced blockade of BUNV infection. Considering that the Na^+/K^+ ATPase is a promising pharmacological target in viral infections, future work will be necessary to study in detail how digoxin and similar compounds work. Even for those antiviral compounds that do not reach a clinical setting, their characterization will help to increase our knowledge on virus–host interactions and to unveil novel therapeutic targets.

Funding information
This work was supported by grants BIO2015-68758-R and RTI2018-094445-B-I00 (MCI/AEI/FEDER, UE) (to C.R.). A.F.-O. has been the recipient of a fellowship for PhD students (FPI Programme) from the Ministry of Science and Innovation of Spain. B.P. has been recipient of a post-doctoral contract from the CNB - Severo Ochoa Centres of Excellence Programme. The funders had no role in study design, data collection and interpretation, decision to publish, or preparation of the manuscript.

Acknowledgements
We thank the late Dr Richard M. Elliott for providing the rBUNGc-eGFP virus, the rabbit polyclonal antiserum against BUNV particles, and the mouse monoclonal antibody Mab742 specific for BUNV Gc protein. We are grateful to Sylvia Gutiérrez-Erlandsson and Ana Oña (from the CNB advanced light microscopy core facility), and Carmen Moreno-Ortiz and Sara Escudero (from the CNB flow cytometry core facility) for support with confocal microscopy and flow cytometry, respectively.

Author contributions
This study was conceived and designed by B.P. and C.R. B.P., A.F.O. and M.G.S. performed experiments. B.P., A.F.O. M.G.S. and C.R. analyzed data. B.P. wrote the initial draft of the manuscript. All authors read, edited and approved the manuscript.

Conflicts of interest
The authors declare that there are no conflicts of interest.

References

1. Feldmann H, Sprecher A, Geisbert TW. Ebola. *N Engl J Med* 2020;382:1832–1842.
2. Gowen BB, Hickerson BT. Hemorrhagic fever of bunyavirus etiology: disease models and progress towards new therapies. *J Microbiol* 2017;55:183–195.
3. Howard CR, Fletcher NF. Emerging virus diseases: can we ever expect the unexpected? *Emerg Microbes Infect* 2012;1:e46.
4. Petersen E, Koopmans M, Go U, Hamer DH, Petrosillo N, *et al*. Comparing SARS-CoV-2 with SARS-CoV and influenza pandemics. *Lancet Infect Dis* 2020;20:e238–e244.
5. Silva NM, Santos NC, Martins IC. Dengue and zika viruses: epidemiological history, potential therapies, and promising vaccines. *TropicalMed* 2020;5:150.
6. Spengler JR, Estrada-Peña A, Garrison AR, Schmaljohn C, Spiropoulou CF, *et al*. A chronological review of experimental infection studies of the role of wild animals and livestock in the maintenance and transmission of Crimean-Congo hemorrhagic fever virus. *Antiviral Research* 2016;135:31–47.
7. Sutton TC. The pandemic threat of emerging H5 and H7 avian influenza viruses. *Viruses* 2018;10:461.
8. Takayama-Ito M, Saijo M. Antiviral drugs against severe fever with thrombocytopenia syndrome virus infection. *Front Microbiol* 2020;11:150.
9. Geraghty RJ, Aliota MT, Bonnac LF. Broad-spectrum antiviral strategies and nucleoside analogues. *Viruses* 2021;13:667.
10. Bauer L, Lyoo H, van der Schaar HM, Strating JR, van Kuppeveld FJ. Direct-acting antivirals and host-targeting strategies to combat enterovirus infections. *Curr Opin Virol* 2017;24:1–8.
11. D'Ambrosio R, Degasperi E, Colombo M, Aghemo A. Direct-acting antivirals: the endgame for hepatitis C? *Curr Opin Virol* 2017;24:31–37.
12. García-Serradilla M, Risco C, Pacheco B. Drug repurposing for new, efficient, broad spectrum antivirals. *Virus Res* 2019;264:22–31.
13. Parlati L, Pol S. Direct acting antivirals failure: cause and retreatment options. *Expert Rev Gastroenterol Hepatol* 2018;12:1245–1250.
14. Bekerman E, Einav S. Infectious disease. Combating emerging viral threats. *Science* 2015;348:282–283.
15. Martinez JP, Sasse F, Brönstrup M, Diez J, Meyerhans A. Antiviral drug discovery: broad-spectrum drugs from nature. *Nat Prod Rep* 2015;32:29–48.
16. Mercorelli B, Palù G, Loregian A. Drug repurposing for viral infectious diseases: How Far Are We? *Trends Microbiol* 2018;26:865–876.
17. Nosengo N. Can you teach old drugs new tricks? *Nature* 2016;534:314–316.
18. Hirsch AJ. The use of RNAi-based screens to identify host proteins involved in viral replication. *Future Microbiol* 2010;5:303–311.
19. Puschnik AS, Majzoub K, Ooi YS, Carette JE. A CRISPR toolbox to study virus-host interactions. *Nat Rev Microbiol* 2017;15:351–364.
20. Götte M. Remdesivir for the treatment of Covid-19: the value of biochemical studies. *Curr Opin Virol* 2021;49:81–85.
21. Barrows NJ, Campos RK, Powell ST, Prasanth KR, Schott-Lerner G, *et al*. A screen of FDA-approved drugs for inhibitors of zika virus infection. *Cell Host Microbe* 2016;20:259–270.
22. Mei M, Tan X. Current strategies of antiviral drug discovery for COVID-19. *Front Mol Biosci* 2021;8.
23. García-Serradilla M, Risco C. Light and electron microscopy imaging unveils new aspects of the antiviral capacity of silver nanoparticles in bunyavirus-infected cells. *Virus Res* 2021;302:198444.
24. Sachse M, Fernández de Castro I, Tenorio R, Risco C. The viral replication organelles within cells studied by electron microscopy. *Adv Virus Res* 2019;105:1–33.
25. Sachse M, Tenorio R, Fernández de Castro I, Muñoz-Basagoiti J, Perez-Zsolt D, *et al*. Unraveling the antiviral activity of plitidepsin against SARS-CoV-2 by subcellular and morphological analysis. *Antiviral Res* 2022;200:105270.
26. Ter Horst S, Conceição-Neto N, Neyts J, Rocha-Pereira J. Structural and functional similarities in bunyaviruses: perspectives for pan-bunya antivirals. *Rev Med Virol* 2019;29:e2039.
27. Madrid PB, Chopra S, Manger ID, Gilfillan L, Keepers TR, *et al*. A systematic screen of FDA-approved drugs for inhibitors of biological threat agents. *PLoS One* 2013;8:e60579.
28. Salanueva IJ, Novoa RR, Cabezas P, López-Iglesias C, Carrascosa JL, *et al*. Polymorphism and structural maturation of bunyamwera virus in Golgi and post-Golgi compartments. *J Virol* 2003;77:1368–1381.
29. Watret GE, Pringle CR, Elliott RM. Synthesis of bunyavirus-specific proteins in a continuous cell line (XTC-2) derived from *Xenopus laevis*. *J Gen Virol* 1985;66 (Pt 3):473–482.
30. Shi X, van Mierlo JT, French A, Elliott RM. Visualizing the replication cycle of *Bunyamwera Orthobunyavirus* expressing fluorescent protein-tagged Gc glycoprotein. *J Virol* 2010;84:8460–8469.
31. Lappin DF, Nakitare GW, Palfreyman JW, Elliott RM. Localization of *Bunyamwera bunyavirus* G1 glycoprotein to the Golgi requires association with G2 but not with NSm. *J Gen Virol* 1994;75 (Pt 12):3441–3451.
32. Fontana J, López-Montero N, Elliott RM, Fernández JJ, Risco C. The unique architecture of Bunyamwera virus factories around the Golgi complex. *Cell Microbiol* 2008;10:2012–2028.
33. Tolosa L, Donato MT, Gómez-Lechón MJ. General cytotoxicity assessment by means of the MTT assay. *Methods Mol Biol* 2015;1250:333–348.
34. Fernández de Castro I, Tenorio R, Ortega-González P, Knowlton JJ, Zamora PF, *et al*. A modified lysosomal organelle mediates nonlytic egress of reovirus. *J Cell Biol* 2020;219:e201910131.
35. Tenorio R, Fernández de Castro I, Knowlton JJ, Zamora PF, Lee CH, *et al*. Reovirus σNS and μNS proteins remodel the endoplasmic reticulum to build replication neo-organelles. *mBio* 2018;9:e01253-18.
36. Shah NR, Sunderland A, Grdzelishvili VZ. Cell type mediated resistance of vesicular stomatitis virus and Sendai virus to ribavirin. *PLoS One* 2010;5:e11265.
37. Shi X, Goli J, Clark G, Brauburger K, Elliott RM. Functional analysis of the *Bunyamwera orthobunyavirus* Gc glycoprotein. *J Gen Virol* 2009;90:2483–2492.
38. Ren N, Wang F, Zhao L, Wang S, Zhang G, *et al*. Efficient rescue of a newly classified Ebinur lake orthobunyavirus with GFP reporter and its application in rapid antiviral screening. *Antiviral Res* 2022;207:105421.
39. Shi X, Elliott RM. Generation and analysis of recombinant *Bunyamwera orthobunyaviruses* expressing V5 epitope-tagged L proteins. *J Gen Virol* 2009;90:297–306.
40. Fan Y, Sanyal S, Bruzzone R. Breaking bad: how viruses subvert the cell cycle. *Front Cell Infect Microbiol* 2018;8:396.
41. Ahuja D, Sáenz-Robles MT, Pipas JM. SV40 large T antigen targets multiple cellular pathways to elicit cellular transformation. *Oncogene* 2005;24:7729–7745.
42. Ashbrook AW, Lentscher AJ, Zamora PF, Silva LA, May NA, *et al*. Antagonism of the sodium-potassium ATPase impairs Chikungunya virus infection. *mBio* 2016;7:e00693-16.
43. Gupta RS, Chopra A, Stetsko DK. Cellular basis for the species differences in sensitivity to cardiac glycosides (digitalis). *J Cell Physiol* 1986;127:197–206.
44. Keenan SM, DeLisle RK, Welsh WJ, Paula S, Ball WJ. Elucidation of the Na+, K+-ATPase digitalis binding site. *J Mol Graph Model* 2005;23:465–475.
45. Cho J, Lee YJ, Kim JH, Kim SI, Kim SS, *et al*. Antiviral activity of digoxin and ouabain against SARS-CoV-2 infection and its implication for COVID-19. *Sci Rep* 2020;10:16200.
46. Jeon S, Ko M, Lee J, Choi I, Byun SY, *et al*. Identification of antiviral drug candidates against SARS-CoV-2 from FDA-approved drugs. *Antimicrob Agents Chemother* 2020;64:e00819-20.
47. Kapoor A, Cai H, Forman M, He R, Shamay M, *et al*. Human cytomegalovirus inhibition by cardiac glycosides: evidence for involvement of the HERG gene. *Antimicrob Agents Chemother* 2012;56:4891–4899.

48. Laird GM, Eisele EE, Rabi SA, Nikolaeva D, Siliciano RF. A novel cell-based high-throughput screen for inhibitors of HIV-1 gene expression and budding identifies the cardiac glycosides. *J Antimicrob Chemother* 2014;69:988–994.
49. Wong RW, Balachandran A, Ostrowski MA, Cochrane A. Digoxin suppresses HIV-1 replication by altering viral RNA processing. *PLoS Pathog* 2013;9:e1003241.
50. Ianevski A, Yao R, Biza S, Zusinaite E, Mannik A, *et al*. Identification and tracking of antiviral drug combinations. *Viruses* 2020;12:1178.
51. Saul S, Einav S. Old drugs for a new virus: repurposed approaches for combating COVID-19. *ACS Infect Dis* 2020;6:2304–2318.
52. Amarelle L, Lecuona E. The Antiviral Effects of Na,K-ATPase Inhibition: A Minireview. *Int J Mol Sci* 2018;19:2154.
53. Baer A, Austin D, Narayanan A, Popova T, Kainulainen M, *et al*. Induction of DNA damage signaling upon Rift Valley fever virus infection results in cell cycle arrest and increased viral replication. *J Biol Chem* 2012;287:7399–7410.
54. Elliott RM, Weber F. Bunyaviruses and the type I interferon system. *Viruses* 2009;1:1003–1021.
55. Weber F, Dunn EF, Bridgen A, Elliott RM. The Bunyamwera virus nonstructural protein NSs inhibits viral RNA synthesis in a minireplicon system. *Virology* 2001;281:67–74.
56. Wuerth JD, Weber F. Phleboviruses and the type I interferon response. *Viruses* 2016;8:174.
57. Risco C, de Castro IF, Sanz-Sánchez L, Narayan K, Grandinetti G, *et al*. Three-dimensional imaging of viral infections. *Annu Rev Virol* 2014;1:453–473.
58. Li X, Wu K, Zeng S, Zhao F, Fan J, *et al*. Viral infection modulates mitochondrial function. *Int J Mol Sci* 2021;22:4260.
59. Novoa RR, Calderita G, Arranz R, Fontana J, Granzow H, *et al*. Virus factories: associations of cell organelles for viral replication and morphogenesis. *Biol Cell* 2005;97:147–172.
60. Ren Z, Zhang X, Ding T, Zhong Z, Hu H, *et al*. Mitochondrial dynamics imbalance: a strategy for promoting viral infection. *Front Microbiol* 2020;11:1992.
61. Fernández de Castro I, Tenorio R, Risco C. Virus factories. In: Bamford DH and Zuckerman M (eds). *Encyclopedia of Virology*, 4th edn, vol. 1. Oxford: Academic Press; 2021. pp. 495–500.
62. Hackenbrock CR. Ultrastructural bases for metabolically linked mechanical activity in mitochondria. I. Reversible ultrastructural changes with change in metabolic steady state in isolated liver mitochondria. *J Cell Biol* 1966;30:269–297.
63. Hackenbrock CR. Ultrastructural bases for metabolically linked mechanical activity in mitochondria. II. Electron transport-linked ultrastructural transformations in mitochondria. *J Cell Biol* 1968;37:345–369.
64. Valcarce C, Navarrete RM, Encabo P, Loeches E, Satrústegui J, *et al*. Postnatal development of rat liver mitochondrial functions. The roles of protein synthesis and of adenine nucleotides. *J Biol Chem* 1988;263:7767–7775.
65. Zhang L, Qin Y, Chen M. Viral strategies for triggering and manipulating mitophagy. *Autophagy* 2018;14:1665–1673.
66. Lopez-Mejia IC, Fajas L. Cell cycle regulation of mitochondrial function. *Curr Opin Cell Biol* 2015;33:19–25.
67. Mitra K, Wunder C, Roysam B, Lin G, Lippincott-Schwartz J. A hyperfused mitochondrial state achieved at G1-S regulates cyclin E buildup and entry into S phase. *Proc Natl Acad Sci* 2009;106:11960–11965.
68. Ghebrehiwet B, Lim BL, Kumar R, Feng X, Peerschke EI. gC1q-R/p33, a member of a new class of multifunctional and multicompartmental cellular proteins, is involved in inflammation and infection. *Immunol Rev* 2001;180:65–77.
69. Nesher M, Shpolansky U, Rosen H, Lichtstein D. The digitalis-like steroid hormones: new mechanisms of action and biological significance. *Life Sci* 2007;80:2093–2107.
70. Skou JC, Esmann M. The Na,K-ATPase. *J Bioenerg Biomembr* 1992;24:249–261.
71. Fuerstenwerth H. On the differences between ouabain and digitalis glycosides. *Am J Ther* 2014;21:35–42.
72. Li Q, Pogwizd SM, Prabhu SD, Zhou L. Inhibiting Na+/K+ ATPase can impair mitochondrial energetics and induce abnormal Ca2+ cycling and automaticity in guinea pig cardiomyocytes. *PLoS One* 2014;9:e93928.
73. Kaasik A, Safiulina D, Zharkovsky A, Veksler V. Regulation of mitochondrial matrix volume. *Am J Physiol Cell Physiol* 2007;292:C157–63.
74. Shalbuyeva N, Brustovetsky T, Bolshakov A, Brustovetsky N. Calcium-dependent spontaneously reversible remodeling of brain mitochondria. *J Biol Chem* 2006;281:37547–37558.
75. Charlton FW, Hover S, Fuller J, Hewson R, Fontana J, *et al*. Cellular cholesterol abundance regulates potassium accumulation within endosomes and is an important determinant in bunyavirus entry. *J Biol Chem* 2019;294:7335–7347.
76. Hover S, Foster B, Fontana J, Kohl A, Goldstein SAN, *et al*. Bunyavirus requirement for endosomal K+ reveals new roles of cellular ion channels during infection. *PLoS Pathog* 2018;14:e1006845.
77. Guo J, Jia X, Liu Y, Wang S, Cao J, *et al*. Screening of natural extracts for inhibitors against Japanese encephalitis virus infection. *Antimicrob Agents Chemother* 2020;64:e02373-19.
78. Xie Z, Askari A. Na(+)/K(+)-ATPase as a signal transducer. *Eur J Biochem* 2002;269:2434–2439.